Kinetics of Catalytic Hydrogenation of 5-Hydroxymethylfurfural to 2,5-bis-Hydroxymethylfuran in Aqueous Solution over Ru/C

ANANDKUMAR B. JAIN, PRAKASH D. VAIDYA

Department of Chemical Engineering, Institute of Chemical Technology, Matunga, Mumbai, 400 019, India

Received 16 October 2015; revised 26 February 2016; accepted 1 March 2016

DOI 10.1002/kin.20992
Published online 28 March 2016 in Wiley Online Library (wileyonlinelibrary.com).

ABSTRACT: 5-Hydroxymethylfurfural (5-HMF) is a cellulosic product of the hydrolysis of biomass, and it is widely considered for the production of several interesting chemicals and derivatives. In the present work, catalytic hydrogenation of 5-hydroxymethylfurfural to 2,5-bis-hydroxymethylfuran was investigated using 5% Ru/C in the aqueous phase. Kinetic data were experimentally obtained over a wide range of temperatures (313–343 K), H_2 partial pressure (0.69–2.07 MPa), initial HMF concentration (19.8–59.5 mM), and catalyst loading (0.3–0.7 kg/m^3) in a three-phase slurry reactor. Disappearance of initial 5-HMF concentrations was modeled using the power law and Langmuir–Hinshelwood–Hougen–Watson models. A model based on the competitive adsorption of molecular H_2 and HMF was proposed. It is presumed that surface reaction between nondissociatively chemisorbed H_2 and 5-HMF was rate determining. This model provided the best fit for the kinetic data. From the Arrhenius equation, the activation energy for the surface reaction was found to be 104.9 kJ/mol. © 2016 Wiley Periodicals, Inc. Int J Chem Kinet 48: 318–328, 2016

INTRODUCTION

Cellulosic biomass compounds such as 5-hydroxymethylfurfural (5-HMF), which show high oxygen–carbon ratio with high chemical functionality, have provided several opportunities to produce chemicals and polymer-building blocks during the past century [1–3]. 5-HMF is a well-known chemical, commonly referred to as the "sleeping giant." It is the dehydration product of fructose in the presence of acid catalyst with levulinic acid as the side product [4,5]. 5-HMF has two functionalities: One is the hydroxyl group, and the other is the carbonyl group attached to the furan ring, which provides high

Correspondence to: P. D. Vaidya; e-mail: pd.vaidya@ictmumbai.edu.in.

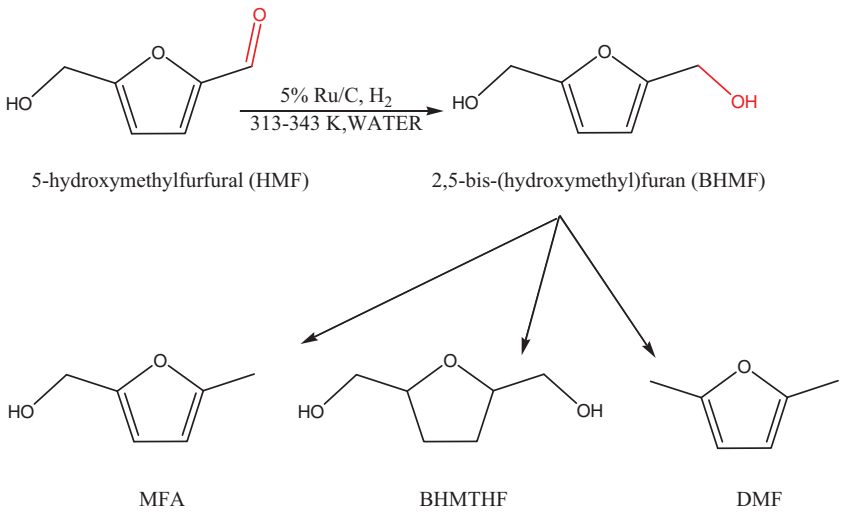

Figure 1 Reaction scheme of 5-HMF hydrogenation to BHMF.

reactivity for the production of valuable chemicals, biofuels, and furan derivatives via oxidation or hydrogenation processes [6]. For example, hydrogenation of 5-HMF produces 2,5-bis-hydroxymethylfuran (BHMF), 2,5-bis-hydroxymethyltetrahydrofuran (BHMTHF), 5-methylfurfuryl alcohol (MFA), and 2,5-dimethylfuran (DMF). It can be used in pharmaceutical intermediates, fine chemicals, dyes, food, resins, polymers, fuel additives, and fibers industries [7–12].

Catalytic hydrogenation of 5-HMF over various metals (Cu, Pd, Ni, Fe, Pt, Rh, and Ru) has been extensively studied [13,14]. The choice of catalyst and reaction variables governs product distribution. For example, DMF is the major product when Ru/C [15–17] and the bimetallic Cu-Ru/C [14,18] are used in nonaqueous media. Contrarily, BHMF is formed in aqueous solution at low temperature (298 K) over Ru-clusters immobilized in nanosized mesoporous zirconium silica [19]. Furthermore, BHMTHF is the preferred product when Ru is supported on ceria, magnesia-zirconia, and γ-alumina, whereas Pt and Pd are less selective than Ru [20]. While Pd promotes the formation of 5-methyl furfural [21], Pt and Ir-Re catalysts are selective to BHMF [22,23].

Kinetics of hydrogenation of biomass-derived compounds in aqueous solution over Ru/C was investigated in our previous works, e.g., hydroxyacetone, hydroxyacetaldehyde, guaiacol, and 2-furanone [24], levoglucosan [25], vanillin [26], and xylenol and maltol [27]. Often, a potential kinetic model was not enough to represent the rate data owing to fractional reaction orders and, consequently, hyperbolic kinetic models were needed in these works. Some other studies focused on ligno-cellulosic biomass, at large, and covered a lumped approach to functional group hydrogenation and hydro-deoxygenation reaction kinetics [28–30]. But so far, there is no information on the mass transfer analysis and kinetic modelling of 5-HMF hydrogenation to BHMF over Ru/C.

Catalytic hydrogenation in water provides a green route for conversion of 5-HMF to BHMF (Fig. 1). In this work, reaction kinetics of 5-HMF hydrogenation in aqueous solution was investigated using the Ru/C catalyst in a slurry reactor. Kinetic data were experimentally obtained over a wide range of temperatures (313–343 K), H_2 partial pressure (0.69–2.07 MPa), initial 5-HMF concentration (19.8–59.5 mM), and catalyst loading (0.3–0.7 kg/m^3). The initial rates for the disappearance of 5-HMF were fitted to a kinetic model, which presumed that the surface reaction between nondissociatively chemisorbed H_2 and 5-HMF is rate determining. From the temperature dependence of the surface reaction rate constant, the activation energy was found to be very high (104.9 kJ/mol), which indicated that the reaction conditions are favorable for studying reaction kinetics.

EXPERIMENTAL

Materials

5-Hydroxymethylfurfural (5-HMF; 98%) was purchased from Sigma Aldrich (Mumbai, India). Hydrogen (H_2) and nitrogen (N_2) cylinders (99.9%) were purchased from Inox Air Products (Mumbai, India). A commercial 5% Ru/C catalyst was supplied by

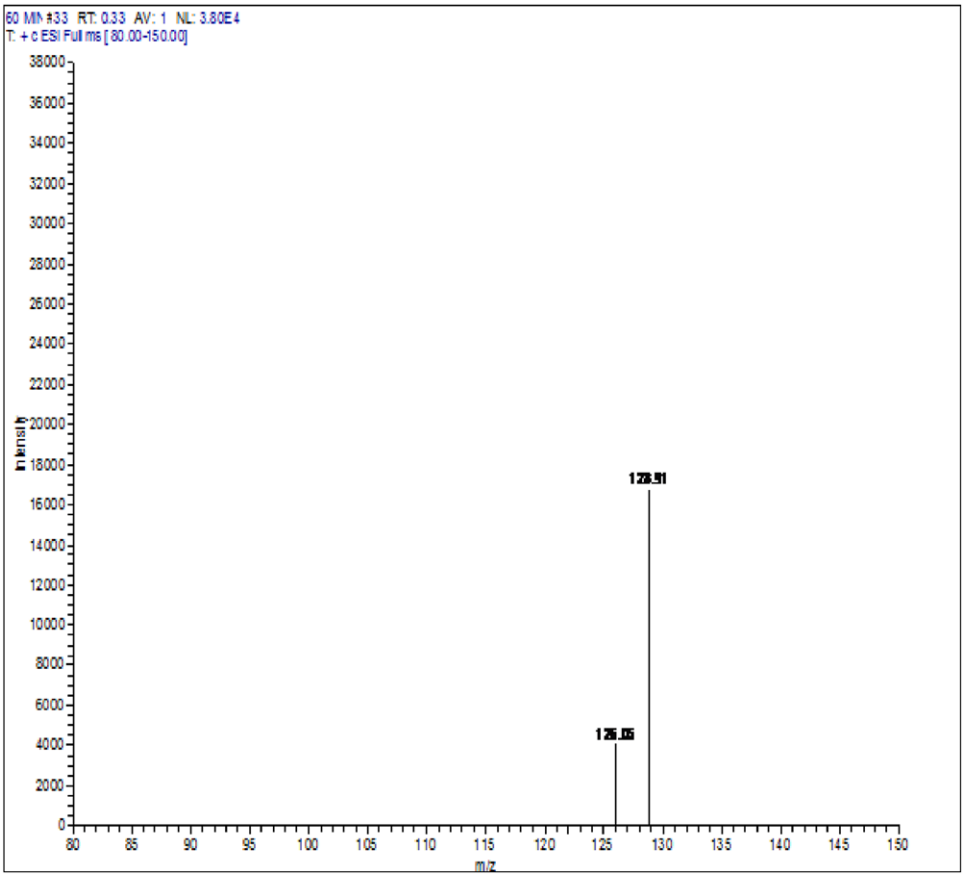

Figure 2 MS data to confirm the formation of BHMF.

Arora-Matthey. To probe any possible influence of the modifier Cu on the performance of Ru/C, a bimetallic Cu-Ru/C (3:1) catalyst was prepared by using incipient wetness impregnation method [18].

Methods and Analysis

The experimental setup was earlier discussed in previous works [24–27]. In this work, we investigated kinetics in the 313–343 K range at different H_2 partial pressures (0.69–2.07 MPa) and catalyst concentrations (0.3–0.7 kg/m^3). 5-HMF was converted to BHMF in the 313–343 K range. Few runs were conducted at high temperature ($T \geq 373$ K) to just ascertain possible formation of by-products. When the temperature was increased beyond 373 K, 5-HMF and BHMF were converted to BHMTHF, MFA, and DMF. The fall in the 5-HMF concentration was recorded using 5 mM H_2SO_4 mobile phase by a refractive index (RI) detector and HPLC technique (Agilent Technologies). As evident from liquid chromatography–mass spectrometry (LC–MS) results, 5-HMF was converted to BHMF (see Fig. 2). From total organic carbon analysis (ANATOC Instruments), it was found that the carbon balance was 98%. The reproducibility of results, in terms of analysis, was checked, and the error in experimental measurements was <3%.

Catalyst Characterization

To study the surface morphology of the catalyst, the scanning-electron microscopy (SEM) technique was used. Powder X-ray diffraction (XRD) patterns of the fresh and spent catalyst were obtained using a Rigaku Miniflex D 500 diffractometer and monochromic Cu Kα radiation (XRD Commander). The instrument parameters were set at 25 mA, 40 kV, scan speed at 0.1 s^{-1}, increment 0.01, and spinner rotation 5. The mean catalyst particle size (21.7 μm) was measured using a Coulter LS 230 particle size analyzer. Surface metallic atom characteristics such as dispersion ($D = 0.028$) and active particle diameter (94 nm) were investigated by H_2 chemisorption (Micromeritics 2920 unit). Procedures for BET analysis of Ru/C,

determination of turnover frequency and confirmation of the existence of a chemical control regime were described in our previous work [27] and used here.

RESULTS AND DISCUSSION

As shown in Fig. 1, 5-HMF is hydrogenated over Ru/C to BHMF in aqueous-phase. BHMF can be further reduced to BHMTHF, MFA, and DMF. Product distribution depends on the reaction conditions, solvent, and catalyst selection. In the present work, we used mild aqueous-phase reaction conditions for the fully selective hydrogenation of 5-HMF to BHMF. Further conversion of BHMF to other products was not observed in the lower temperature range 313–343 K. 5-HMF was fully converted to BHMF (selectivity 100%). The balance of 5-HMF and BHMF per the initial 100% 5-HMF was satisfactory (98%).

We observed that the selectivity of BHMF decreased when reaction conditions were intensified ($T \geq$ 373 K). We also observed that the yield of DMF increases when the Cu-Ru/C catalyst was used at high temperature in 5-HMF hydrogenation. Hence, we maintained lower temperature reaction conditions using 5% Ru/C in aqueous-phase hydrogenation of 5-HMF to BHMF.

SEM images for fresh and spent Ru/C are shown in Figs. 3a and 3b. It is evident that the honeycomb monolithic structure of the catalyst (seen in Fig. 3a) was retained even after reaction (Fig. 3b). SEM image of Cu-Ru/C is shown in Fig. 4a, whereas the results of EDX analysis are shown in Fig. 4b. The concentration of Ru (0.99 ppm) and Cu (2.88 ppm) was measured by the ICP-OES instrument. Both the fresh and spent Ru/C samples showed a similar XRD pattern (see Fig. 5). Diffraction peaks of Ru^0 species were observed ($2\theta = 37°$ and 43°). The broad peak at 26.8° for carbon suggests that the catalyst is amorphous in nature. Interestingly, no new intense peak was observed, which may be due to the high dispersion of Ru on the support.

In this section, the effects of reaction variables on 5-HMF conversion and product distribution are discussed. We used different temperatures (T), molecular H_2 partial pressures P_{H_2}, reactant concentrations (C_{HMF}), and catalyst loadings (ω) as shown in Table I.

Effect of Temperature

The dependency of concentrations of 5-HMF and BHMF on time at 313, 328, and 343 K is represented in Fig. 6. In all experiments, the reaction variables used were as follows: $P_{H_2} = 0.69$ MPa, $C_{HMF,0} = 39.7$ mM, and $\omega = 0.5$ kg/m^3. At $T = 343$ K, the highest

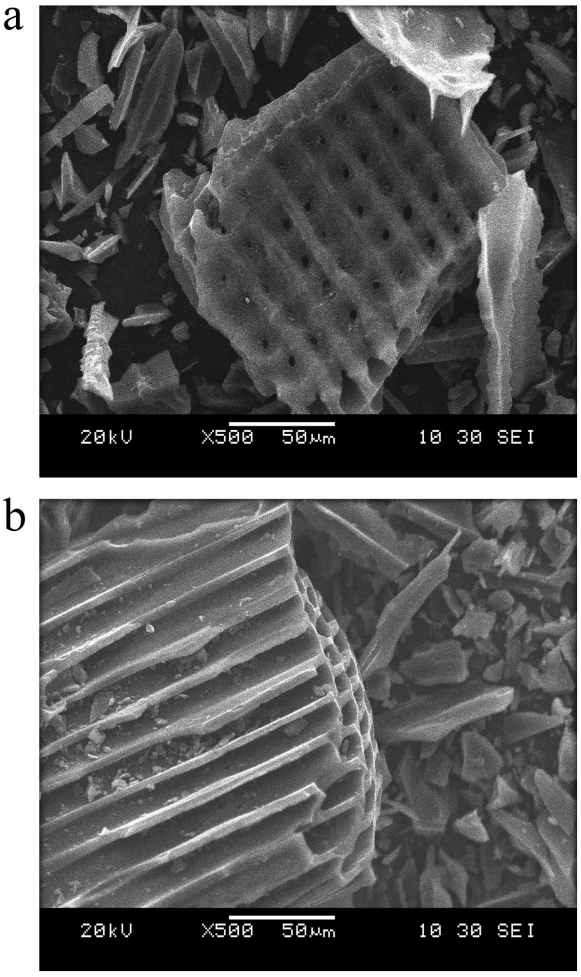

Figure 3 SEM image of (a) the fresh and (b) spent Ru/C catalyst.

conversion after 60 min was 48.5%. Interestingly, the concentration vs. time curve showed a distinct trend at all temperatures. The reaction proceeded rapidly at the beginning, so that unexpectedly high rate of conversion was observed within the first 5 min; thereafter, a gradual decrease in the rate and, finally, equilibrium-type behavior around 60 min was seen. The reaction of 5-HMF hydrogenation was earlier reported in the literature by many research groups. Some of the earlier studies include the work done by [1,13–18] and [21]. A comparison is given in Table II. Interestingly, Op De Beeck et al. [1] reported complete conversion of 5-HMF to BHMF using the Ru/C catalyst at $T = 333$ K, $P_{H_2} = 5$ MPa in water. Scholz et al. [13] investigated continuous transfer hydrogenolysis of 5-HMF in isopropanol over Pd/Fe_2O_3 at $T = 453$ K, $P_{H_2} =$ 2.5 MPa achieving 100% conversion; the yield of BHMF decreasing with time. In addition to this, Tamura et al. [23] reported 99% yield of BHMF in

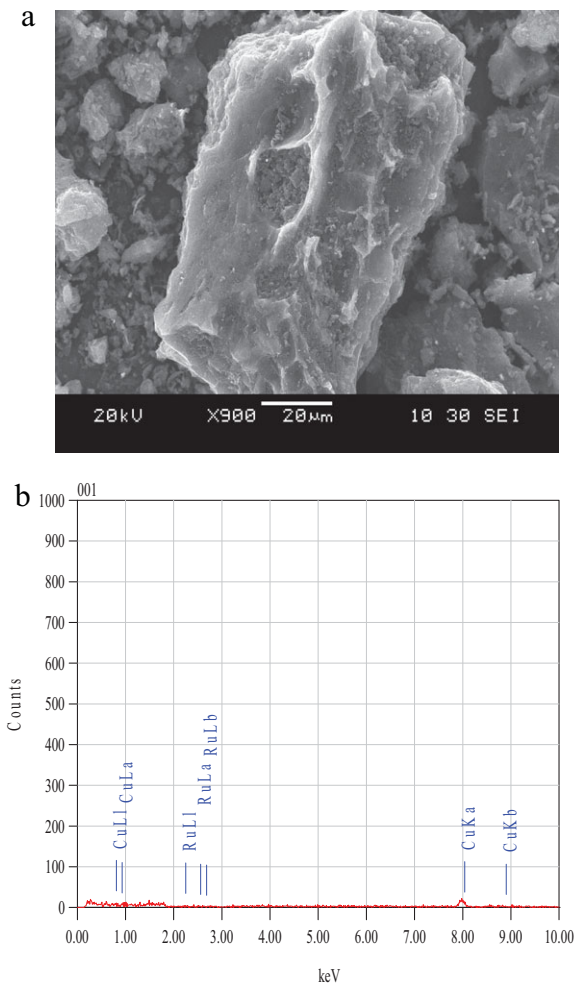

Figure 4 (a) SEM image of the fresh Cu-Ru/C catalyst and (b) results of EDX analysis.

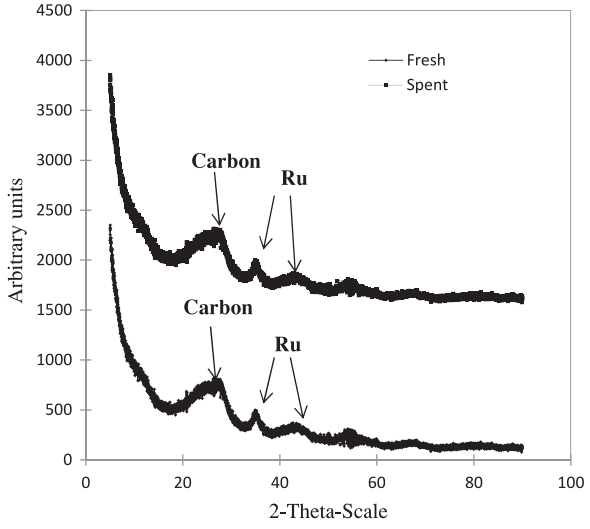

Figure 5 XRD images of fresh and spent Ru/C catalyst.

water at $T = 303$ K and $P_{H_2} = 0.8$ MPa using Ir-ReO_x/SiO_2 with complete conversion of 5-HMF. Chatterjee et al. [22] studied 5-HMF hydrogenation and reported 100% conversion and 98.9% BHMF yield in 2 h at $T = 308$ K, $P_{H_2} = 0.8$ MPa, using Pt/MCM-41 in the aqueous phase.

Effect of Catalyst Loading

The effect of catalyst loading on the initial turnover frequency (TOF) values was investigated at 313, 328, and 343 K in the 0.3–0.7 kg/m^3 range. The values of P_{H_2} and $C_{HMF,0}$ were 0.69 MPa and 39.7 mM, respectively. The results are presented in Table III. With an increase in catalyst loading, the initial rate increased from 4.6×10^{-4} to 10.4×10^{-4} kmol/(m^3 min) at 328 K. Thus, it can be concluded that the reaction rate exhibits first-order dependence on the catalyst concentration.

Effect of H_2 Partial Pressure and Concentration of 5-HMF

The effect of P_{H_2} on the initial TOF values was studied in the range of 0.69 to 2.07 MPa pressure at temperatures 313, 328, and 343 K. While $C_{HMF,0}$ was kept constant at 39.7 mM, a value of catalyst loading $\omega =$ 0.5 kg/m^3 was used. The results are presented in Fig. 7. Clearly, the dependence of initial TOF on P_{H_2} was linear. This behavior suggests that H_2 is weakly adsorbed on the catalyst surface without dissociation. When the H_2 partial pressure was increased threefold from 0.69 to 2.07 MPa at $T = 328$ K, the 5-HMF concentration decreased from 39.7 to 5.1 mM within a period of 1 h. These results are shown in Table I.

The effect of $C_{HMF,0}$ on the initial TOF values was studied at 313, 328, and 343 K in the 19.8–59.5 mM range. The results are depicted in Fig. 8. From the plots of ln r vs. ln $C_{HMF,0}$ (see Fig. 9), the orders of reaction at $T = 313$, 328, and 343 K were found to be equal to 1.15, 1.04, and 0.92, respectively.

Reaction Mechanism and Kinetic Modelling

Langmuir-Hinshelwood-Hougen-Watson (LHHW) kinetics was used for modeling initial rates of 5-HMF disappearance. The hydrogenation reaction of HMF to BHMF was represented as

$$C_6H_6O_3 + H_2 \rightarrow C_6H_8O_3 \qquad (1)$$

Usually, the surface reaction over Ru is the rate-limiting step in the hydrogenation of biomass–precursor compounds in aqueous solution [25–27]. Assuming that the surface reaction between 5-HMF and

Table I Effect of Experimental Conditions on Fractional Conversion (X) of 5-HMF and Turnover Frequency (TOF) Values

$C_{HMF,0}$ (mM)	P_{H_2} (MPa)	Catalyst Loading (ω) kg/m^3	T (K)	Fractional HMF Conversion (X)	TOF (1/min)
19.8	0.69	0.5	313	0.48	1.98
			328	0.70	2.78
			343	0.94	3.97
39.7	0.69	0.5	313	0.34	3.97
			328	0.43	5.41
			343	0.48	7.72
59.5	0.69	0.5	313	0.31	5.77
			328	0.33	8.22
			343	0.44	10.82
39.7	1.38	0.5	313	0.47	8.30
			328	0.69	12.99
			343	0.76	19.48
39.7	2.07	0.5	313	0.66	12.99
			328	0.87	20.06
			343	0.95	28.14

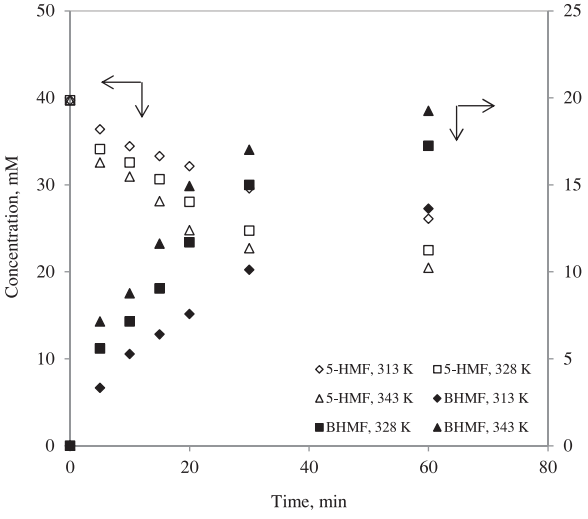

Figure 6 Dependency of concentrations of 5-HMF and BHMF on time at 313, 328 and 343 K ($C_{HMF,0} = 39.7$ mM, $P_{H_2} = 0.69$ MPa and $\omega = 0.5$ kg/m^3).

H_2 is rate controlling, four kinetic models (competitive and noncompetitive) were considered.

Using the sequence of steps reported by us earlier [25], the competitive adsorption of dissociatively chemisorbed H_2 and the reactant is represented as

$$H_2 + 2\,S \overset{k_1, k_{-1}}{\longleftrightarrow} 2\,HS \tag{2}$$

$$HMF + S \overset{k_2, k_{-2}}{\longleftrightarrow} HMFS \tag{3}$$

The surface reaction may be represented as:

$$2HS + HMFS \overset{k_3, k_{-3}}{\longleftrightarrow} BHMF + 3\,S \tag{4}$$

where BHMF is the product. For the case of molecular adsorption of H_2, Eq. (2) is replaced by

$$H_2 + S \overset{k_1, k_{-1}}{\longleftrightarrow} H_2S \tag{5}$$

The surface reaction is now represented by

$$H_2S + HMFS \overset{k_3, k_{-3}}{\longleftrightarrow} BHMF + 2\,S \tag{6}$$

The various steps for noncompetitive adsorption of dissociatively chemisorbed H_2 and HMF are given by

$$H_2 + 2\,S_1 \overset{k_1, k_{-1}}{\longleftrightarrow} 2\,HS_1 \tag{7}$$

$$HMF + S_2 \overset{k_2, k_{-2}}{\longleftrightarrow} HMFS_2 \tag{8}$$

For this case, the surface reaction is given by

$$2HS_1 + HMFS_2 \overset{k_3, k_{-3}}{\longleftrightarrow} BHMF + 2\,S_1 + S_2 \tag{9}$$

For the case of molecular adsorption of H_2, Eq. (7) is replaced by

$$H_2 + S_1 \overset{k_1, k_{-1}}{\longleftrightarrow} H_2S_1 \tag{10}$$

Table II Comparison of this Study with Previous Works on Hydrogenation of 5-HMF[a]

Compound	Reaction Conditions	Products Identified	X (%)	Comment	Reference
5-HMF (39.7 mM)	328 K, 1 h, 0.69 MPa, 5% Ru/C, Solvent: H_2O	BHMF	43	Batch reactor, low temperature, selective hydrogenation of carbonyl group	This work
5-HMF (39.7 mM)	423 K, 0.69 MPa, 5% Ru/C, Solvent: H_2O	BHMF, BHMTHF, MFA, DMF	82	Batch reactor, high temperature reaction conditions, formation of different products	This work
5-HMF (5.6 mmol)	333 K, 40 min, 5 MPa, Ru/C, Solvent: H_2O	BHMF	100	Batch reactor, high pressure reaction	Op De Beeck et al. [1]
5-HMF (0.12 M)	453 K, 25 min, Pd/Fe_2O_3, 2.5 MPa, Solvent: IPA	BHMF, DMF	100	Flow reactor, high temperature and pressure, organic solvent	Scholz et al. [13]
5-HMF (2.5 wt%)	473 K, 2 h, 2 MPa, Ru/C Solvent: THF	DMF	100	Batch reactor, high temperature, organic solvent	Hu et al. [16]
5-HMF (2.5 g 5-HMF)	493 K, 10 h, 0.68 MPa, Cu-Ru/C (3:1); Solvent: 1-butanol	DMF	100	Batch reactor, high temperature, organic solvent	Román- Leshkov et al. [14]
Crude 5-HMF (untreated corn stover)	493 K, 10 h, H_2(g), Cu-Ru/C, solvent: 1-butanol	DMF	–	High temperature, organic solvent	Binder and Raines [18]
5-HMF (6 wt%)	533 K, 1.5 h, $H_2$4.48×10^{-2} mol/g, Ru/C, Solvent: 1-butanol	DMF	99.8	High temperature, organic solvent	Zhang et al. [15]
5-HMF (126 mg)	393 K, 1 h, 6.2 MPa, Pd/C Solvent: ionic liquid	MF, MFA, BHMF, DMF, HD, MTHFA	19	High temperature and pressure required, formation of different products	Chidambaram and Bell [21]
5-HMF (1.2 wt%)	463 K, 6 h, Ru/C, 2 MPa Solvent: IPA	DMF, BHMF, MFA, MF	100	High temperature and pressure required, formation of different products, catalytic transfer hydrogenation	Jae et al. [17]

[a] Abbreviation: BHMF, 2,5-bis-hydroxymethylfuran; BHMTHF, 2,5-bis-hydroxymethyltetrahydrofuran; DMF, 2,5-dimethylfuran; HD, 2,5-dexadione; 5-HMF, 5-hydroxymethylfurfural; MF, 5-methylfurfural; MFA, 5-methylfurfuryl alcohol; MTHFA, 5-methyltetrahydrofurfuryl alcohol; X, fractional conversion.

and the surface reaction is now represented by

$$H_2S_1 + HMFS_2 \overset{k_3, k_{-3}}{\longleftrightarrow} BHMF + S_1 + S_2 \quad (11)$$

Table IV presents the kinetic models (I–IV) and their rate-determining steps (i.e., Eqs. (6), (4), (9) and (11)). All models were simplified to the initial rate equations. A model discrimination technique was used for selecting the most appropriate model. The model parameters were estimated by using the optimization program POLYMATH 6.0 and the Simplex–Levenberg–Marquardt algorithm. Models 3 and 4 did not provide a good fit of the data and hence were rejected.

The average values of RSS, variance, and coefficient of determination (CoD) for all models are given in Table IV at 313, 328, and 343 K. While the values of CoD for models I and II were very close, kinetic parameters estimated from model II did not fit to the experimental data. However, model I reasonably represented kinetic data. The parity plot for model I is shown in Fig. 10. Indeed, the experimental TOF values are in good agreement with the predicted ones.

Furthermore, model I was validated by a straightforward graphical procedure. If model I holds, a plot of $(C_{HMF,0}/r_0)^{1/2}$ vs. $C_{HMF,0}$ should be linear at constant values of C_{H_2}. Certainly, this plot confirmed that model I was appropriate (see Fig. 11). An intrinsic

Table III Effect of Catalyst Loading (ω) on Initial 5-HMF Disappearance Rates (r_0) and TOF Value ($P_{H_2} = 0.69$ MPa, $C_{HMF,0} = 39.7$ mM)

	$r_0 \times 10^4$ (kmol/(m^3 min))			Initial TOF (1/min)		
ω (kg/m^3)	313 K	328 K	343 K	313 K	328 K	343 K
0.3	3.9	4.6	5.3	4.69	5.53	6.37
0.5	6.46	7.5	8.7	4.66	5.41	6.28
0.7	8.85	10.4	12.1	4.74	5.36	6.24

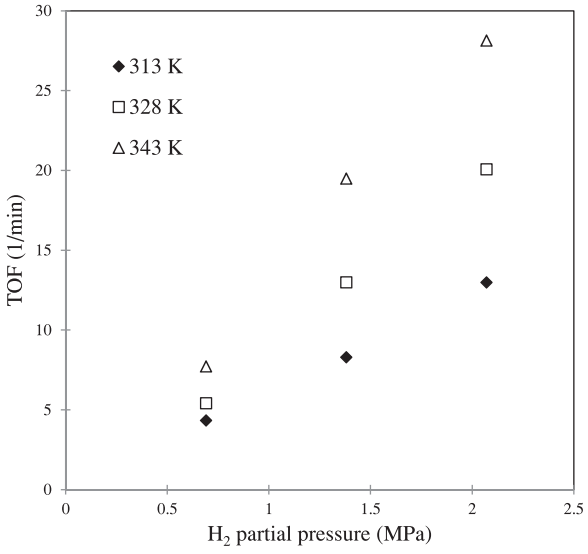

Figure 7 Effect of H_2 partial pressure (P_{H_2}) on the initial TOF values at 313, 328, and 343 K ($C_{HMF,0} = 39.7$ mM and $\omega = 0.5$ kg/m^3).

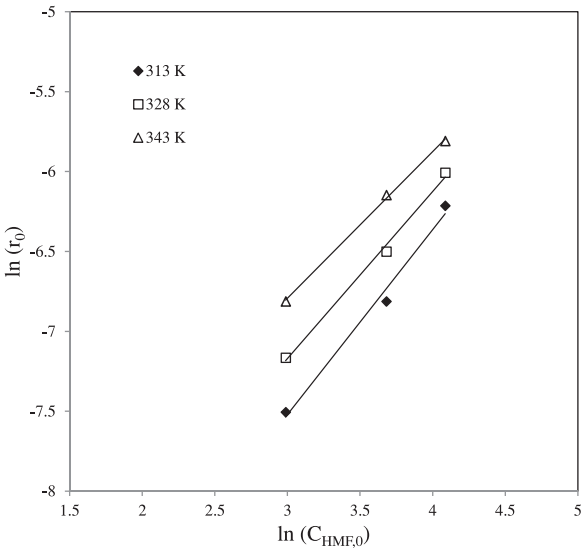

Figure 9 Plots of ln r vs. ln $C_{HMF,0}$ at $T = 313$, 328, and 343 K ($P_{H2} = 0.69$ MPa and $\omega = 0.5$ kg/m^3).

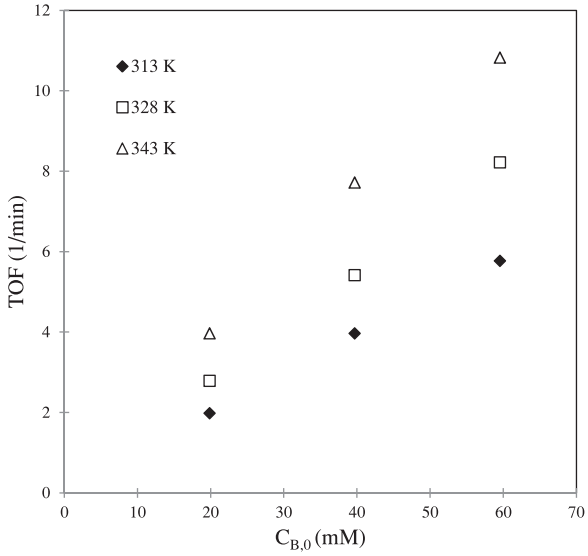

Figure 8 The dependence of the initial TOF on the initial HMF concentration at various temperatures ($P_{H_2} = 0.69$ MPa and $\omega = 0.5$ kg/m^3).

parameter (C_2) method earlier reported by Brahme and Doraiswamy [31] for glucose hydrogenation was used for further discrimination. The proposed models were expressed in terms of either fractional conversion or partial pressure (or concentration). The method involves two different parameters C_1 and C_2. This process describes C_2 in terms of the initial concentration of the reactant. To find out the suitable model from the equation for C_2, the raw data obtained at different initial concentrations of the reactant was used to find the rate at different reaction conditions. Model I ($r_0 = \frac{P(1-X)}{[C_1 - C_2 X]^2}$) can be expressed in terms of C_1 and C_2 as

$$C_1 = \frac{1 + \alpha P K_{H_2} + C_{HMF,0} K_{HMF}}{\left(\alpha\, C_{HMF,0} K_{HMF} K_{H2} k_3\right)^{1/2}} \tag{12}$$

$$C_2 = \frac{K_{HMF}\left(C_{HMF,0}\right)^{1/2}}{\left(\alpha\, K_{HMF} K_{H_2} k_3\right)^{1/2}} \tag{13}$$

Table IV Plausible Kinetic Models (I–IV) and Model Discrimination Parameters for 5-HMF Hydrogenation

Model	Rate-Controlling Step and Initial-Rate Expression	Temperature (K)	Variance	RSS	CoD
I	Eq. (6) $r = \frac{k_3 K_{H_2} K_{HMF} C_{H_2} C_{HMF}}{(1+K_{H_2} C_{H_2}+K_{HMF} C_{HMF})^2}$	313	3.62×10^{-8}	5.38×10^{-5}	0.997
		328	9.50×10^{-8}	8.72×10^{-5}	0.996
		343	2.86×10^{-7}	1.51×10^{-4}	0.994
II	Eq. (4) $r = \frac{k_3 K_{H_2} K_{HMF} C_{H_2} C_{HMF}}{(1+\sqrt{K_{H_2} C_{H_2}}+K_{HMF} C_{HMF})^3}$	313	5.93×10^{-8}	6.89×10^{-5}	0.978
		328	2.00×10^{-7}	1.26×10^{-4}	0.972
		343	4.82×10^{-7}	1.96×10^{-4}	0.967
III	Eq. (9) $r = \frac{k_3 K_{H_2} K_{HMF} C_{H_2} C_{HMF}}{(1+\sqrt{K_{H_2} C_{H_2}})^2(1+K_{HMF} C_{HMF})}$	313	3.38×10^{-8}	5.20×10^{-5}	0.977
		328	9.04×10^{-8}	8.50×10^{-5}	0.961
		343	2.97×10^{-7}	1.54×10^{-4}	0.969
IV	Eq. (11) $r = \frac{k_3 K_{H_2} K_{HMF} C_{H_2} C_{HMF}}{(1+K_{H_2} C_{H_2})(1+K_{HMF} C_{HMF})}$	313	3.99×10^{-8}	5.65×10^{-5}	0.955
		328	1.29×10^{-7}	1.02×10^{-4}	0.941
		343	4.82×10^{-7}	1.96×10^{-4}	0.967

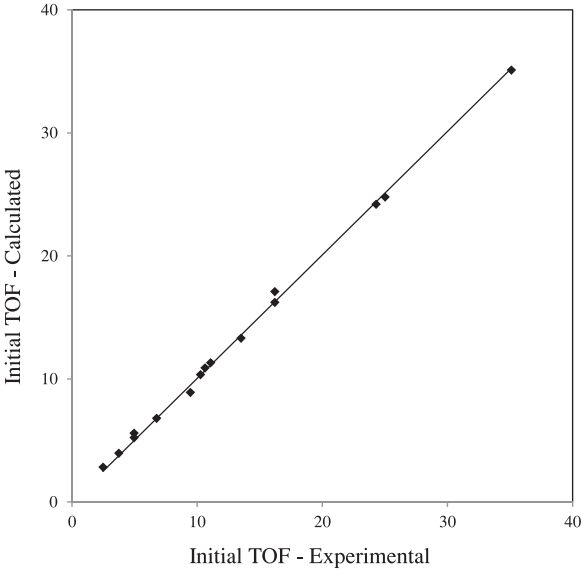

Figure 10 Parity plot for model I.

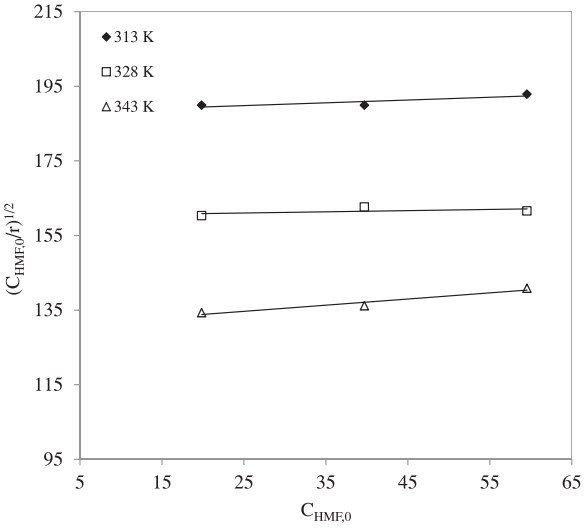

Figure 11 Plots of $(C_{HMF,0}/r_0)^{1/2}$ vs. $C_{HMF,0}$ at $T = 313$, 328, and 343 K.

From Eq. (12) and (13), for the model I, C_2 was calculated from experimental data using the following relation:

$$C_2 = \left(\frac{P}{r_0}\right)^{1/2} \frac{1}{X} - \left(\frac{P(1-X)}{r}\right)^{1/2} \frac{1}{X} \quad (14)$$

Model II $\left(r_0 = \frac{P(1-X)}{[C_1 - C_2 X]^3}\right)$ can be expressed in terms of C_1 and C_2 as follows:

$$C_1 = \frac{1 + (\alpha P K_{H2})^{1/2} + C_{HMF,0} K_{HMF}}{\left(\alpha C_{HMF,0} K_{HMF} K_{H2} k_3\right)^{1/3}} \quad (15)$$

$$C_2 = \frac{K_{HMF} \left(C_{HMF,0}\right)^{1/3}}{(\alpha K_{HMF} K_{H2} k_3)^{1/3}} \quad (16)$$

From Eqs. (15) and (16), for the model II, C_2 was calculated from experimental data using the following relation:

$$C_2 = \left(\frac{P}{r_0}\right)^{1/3} \frac{1}{X} - \left(\frac{P(1-X)}{r}\right)^{1/3} \frac{1}{X} \quad (17)$$

The intrinsic parameter C_2 is a function of $C_{HMF,0}$. At constant values of P, models I and II require plots of

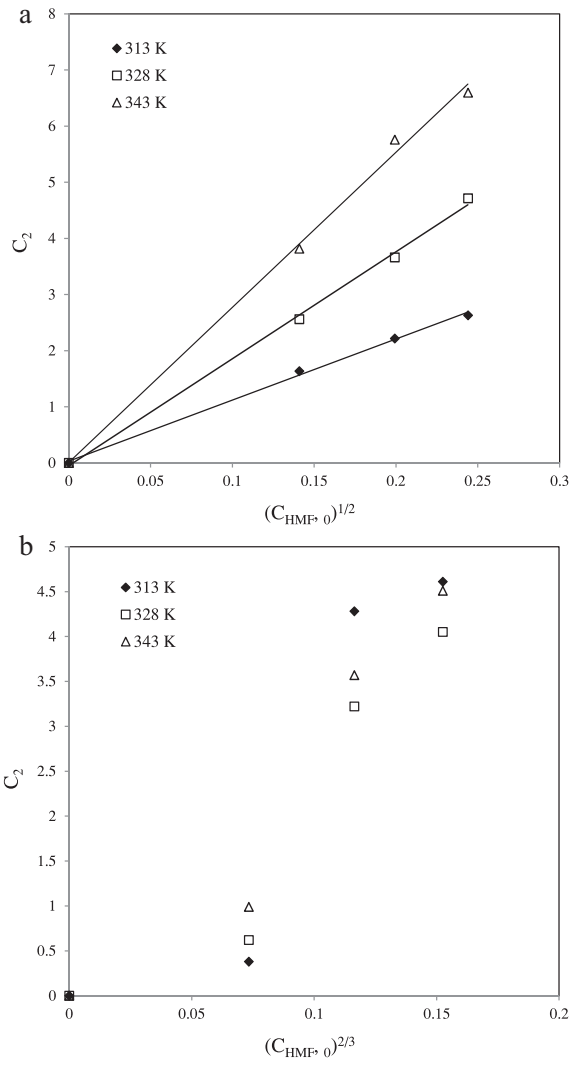

Figure 12 Plots for validation of models I (a) and II (b).

C_2 vs. $C_{HMF,0}^{1/2}$ and C_2 vs. $C_{HMF,0}^{2/3}$ as straight lines passing through the origin. Such graphs for hydrogenation of 5-HMF are shown in Figs. 12a and 12b. Clearly, the plot for model I (i.e., Fig. 11a) is linear with zero intercept. On the other hand, Fig. 11b does not present a linear relation. Thus, model II is ruled out. From the Arrhenius equation, the activation energy for surface reaction of 5-HMF was calculated as 104.9 kJ/mol.

Finally, it may be noted that, among the different mechanistic models considered, model I fits the data well.

CONCLUSIONS

Catalytic hydrogenation in water provides a green route for conversion of 5-HMF to useful chemicals. In the present work, selective hydrogenation and kinetics of 5-HMF to BHMF was studied in a three-phase slurry reactor using the Ru/C catalyst. Using a limited range of temperature, 313–343 K, H_2 partial pressure 0.69–2.07 MPa, initial 5-HMF concentration, 19.8–59.5 mM, and catalyst loading, 0.3–0.7 kg/m^3, kinetic data were experimentally obtained. The apparent reaction orders with respect to 5-HMF and H_2 were close to one. Several LHHW models were proposed to describe reaction kinetics. Using model discrimination techniques, it was found that the kinetic data could be best fitted to a LHHW-based model with surface reaction between competitively adsorbed molecular H_2 and 5-HMF as the rate-controlling step. Finally, it was found that the rise in temperature beyond 373 K resulted in the conversion of 5-HMF and BHMF into BHMTHF, MFA, and DMF. Furthermore, the yield of DMF increased when the Cu-Ru/C catalyst was used at high temperature. These inferences will aid in the designing and operation of hydrogenation reactors for producing useful chemicals from biomass. Also, this work will stimulate further research on hydrogenation kinetics of biomass–precursor compounds in aqueous solution.

NOMENCLATURE

C_2	Intrinsic parameter in Eqs. (12) and (13)
C_{H_2}	Concentration of H_2 in the liquid phase, kmol/m^3
C_{HMF}	Concentration of HMF in the liquid phase, kmol/m^3
$C_{HMF,0}$	Initial concentration of HMF in the liquid phase, kmol/m^3
D	Metal dispersion
K_{HMF}	Adsorption equilibrium constant for HMF, m^3/kmol
K_{H_2}	Adsorption equilibrium constant for H_2, m^3/kmol
k_3	Reaction rate constant, kmol/(kg$_{cat}$ min)
P	Total pressure, atm
P_{H_2}	Partial pressure of H_2, MPa
R^2	Coefficient of determination
r	Rate of reaction, kmol/(kg$_{cat}$ min)
r_0	Initial rate of reaction, kmol/(kg$_{cat}$ min)
S	Active site on catalyst surface
T	Temperature, K
t	Time, h
X	Fractional conversion

GREEK SYMBOLS

α	Henry's law constant, kmol/(m^3 kPa)
ω	Catalyst loading, kg/m^3

Anandkumar B. Jain is grateful to University Grants Commission, New Delhi, India, for financial aid.

BIBLIOGRAPHY

1. Op De Beeck, B., Dusselier, M.; Geboers, J.; Holsbeek, J.; Morré, E.; Oswald, S.; Giebeler, L.; Sels, B. F. Energy Environ Sci 2015, 8, 230–240.
2. Teong, S. P.; Yi, G.; Zhang, Y. Green Chem 2014, 16, 2015–2026.
3. Van Putten, R. J.; Van Dar Wass, J. C.; Jong, E. D.; Rasrendra, C. B.; Heeres, H. J.; de Vries, J. G. Chem Rev 2013, 113, 1499–1597.
4. Tong, X.; Ma, Y.; Li, Y. Appl Catal A: Gen 2010, 385, 1–13.
5. Alonso, D. M.; Bond, J. Q.; Dumesic, J. A. Green Chem 2010, 12, 1493–1513.
6. Kwon, Y.; de Jong, E.; Raoufmoghaddam, S.; Koper, M. T. M. Chem Sus Chem 2013, 6, 1659–1667.
7. Hu, X.; Westerhof, R. J. M.; Wu, L.; Dong, D.; Li, C. Z. Green Chem 2015, 17, 219–224.
8. Gallezot, P. Chem Soc Rev 2012, 41, 1538–1558.
9. Climent, M. J.; Corma, A.; Iborra, S. Green Chem 2011, 13, 520–540.
10. Buntara, T.; Noel, S.; Phua, P. H.; Melián-Cabrera, I.; de Vries, J. G.; Heeres, H. J. Top Catal 2012, 55, 612–619.
11. Climent, M. J.; Corma, A.; Iborra, S. Green Chem 2014, 16, 516–547.
12. Liu, D.; Chen, Y. X. Green Chem 2014, 16, 964–981.
13. Scholz, D.; Aellig, C.; Hermans, I. ChemSusChem 2014, 7, 268–275.
14. Román-Leshkov, Y.; Barrett, C. J.; Liu, Z. Y.; Dumesic, J. A. Science 2007, 447, 982–985.
15. Zhang, J.; Lin, L.; Liu, S. Energy Fuels 2012, 26, 4560–4567.
16. Hu, L.; Tang, X.; Xu, J.; Wu, Z.; Lin, L.; Liu, S. Ind Eng Chem Res 2014, 53, 3056–3064.
17. Jae, J.; Zheng, W.; Lobo, R. F.; Vlachos, D. G. Chem Sus Chem 2013, 6, 1158–1162.
18. Binder, J. B.; Raines, R. T. J Am Chem Soc 2009, 131, 1979–1985.
19. Chen, J.; Lu, F.; Zhang, J.; Yu, W.; Wang, F.; Gao, J.; Xu, J. Chem Cat Chem 2013, 5, 2822–2826.
20. Alamillo, R.; Tucker, M.; Chia, M.; Pagán-Torres, Y.; Dumesic, J. A. Green Chem 2012, 14, 1413–1419.
21. Chidambaram, M.; Bell, A. T. Green Chem 2010, 12, 1253–1262.
22. Chatterjee, M.; Ishizaka, T.; Kawanami, H. Green Chem 2014, 16, 4734–4739.
23. Tamura, M.; Tokonami, K.; Nakagawa, Y.; Tomishige, K. Chem Commun 2013, 49, 7034–7036.
24. Bindwal, A. B.; Bari, A. H.; Vaidya, P. D. Chem Eng J 2012, 207–208, 725–733.
25. Bindwal, A. B.; Vaidya, P. D. Ind Eng Chem Res 2013, 52, 17781–17789.
26. Bindwal, A. B.; Vaidya, P. D. Energy Fuels 2014, 28, 3357–3362.
27. Jain, A. B.; Vaidya, P. D. Energy Fuels 2015, 29, 361–368.
28. Grilc, M.; Lizokar, B. Levec, J. Catal Today 2015, 256, 302–314.
29. Grilc, M.; Lizokar, B. Levec, J. Appl Catal B: Environ 2014, 150–151, 275–287.
30. Grilc, M.; Lizokar, B. Levec, J. Biomass Bioenergy 2014, 63, 300–312.
31. Brahme, P. H.; Doraiswamy, L. K. Ind Eng Chem, Process Des Dev 1976, 15, 130–137.